aerospace

MDPI

Article

Computational Investigations for the Feasibility of Passive Flow Control Devices for Enhanced Aerodynamics of Small-Scale UAVs

Ali Arshad * and Vadims Kovaļčuks

Aeronautics, Space Engineering and Transport Institute, Faculty of Civil and Mechanical Engineering, Riga Technical University, LV-1048 Riga, Latvia; vadims.kovalcuks@rtu.lv
* Correspondence: ali.arshad@rtu.lv

Abstract: The 4R-UAV project aims to develop aerodynamically efficient and environmentally friendly UAVs based on the 4R Circular Economy principle. In this study, the feasibility of the application of PFCDs (Passive Flow Control Devices) was investigated for the small-scale low-speed 4R-UAV wing. The application of PFCDs for small-scale UAV wings is relatively unexplored. Two PFCD types, i.e., MVGs (Micro Vortex Generators) and winglets, were considered for the investigations. In the stepwise investigations, the aerodynamic performance of the MVGs and the winglets was analyzed for the short-span 4R-UAV wing, which was developed from the aerodynamically optimized airfoil SG6043mod. MVGs enhanced the wings near stall properties (especially maximum lift coefficient) and contributed to the delayed wing stall of up to 2°. MVGs manifested the main aerodynamic advantage, which was achieved at the higher angles of attack. Winglets, on the other hand, were found to be extremely effective in cruise conditions with improved pre-stall characteristics. Extensive investigations on winglets were carried out by designing six winglet configurations for the 4R-UAV wing. Blended-type winglets performed well and enhanced pre-stall properties by decreasing the drag (up to 10%) of the wing. The main performance improvement was found in the early angles of attack. In the final step, the combined effect of the integrated PFCDs was analyzed. The final wing (integrated MVGs and winglets) also exhibited enhanced performance with nearly 6% increased lift-to-drag ratio in cruise conditions. The limited aerodynamic advantage achieved from the PFCDs in small-scale UAV applications can be useful in specific (civil or military) missions. Further verifications are planned in the future by means of experimental and flight testing.

Keywords: passive flow control devices; Micro-Vortex Generators (MVGs); winglets; small-scale UAV; CFD

check for updates

Citation: Arshad, A.; Kovaļčuks, V. Computational Investigations for the Feasibility of Passive Flow Control Devices for Enhanced Aerodynamics of Small-Scale UAVs. *Aerospace* **2024**, *11*, 473. https://doi.org/10.3390/aerospace11060473

Academic Editor: Alex Zanotti

Received: 9 April 2024
Revised: 5 June 2024
Accepted: 7 June 2024
Published: 13 June 2024

Copyright: © 2024 by the authors. Licensee MDPI, Basel, Switzerland. This article is an open access article distributed under the terms and conditions of the Creative Commons Attribution (CC BY) license (https://creativecommons.org/licenses/by/4.0/).

1. Introduction

The 4R-UAV project is supported by the Latvian Council of Science to develop aerodynamically efficient, environmentally friendly UAVs. According to the European Commission as part of the European green deal [1], the EU is responsible for 10% of global greenhouse gas emissions and is a worldwide leader in transitioning towards a net-zero-greenhouse gas emissions economy. The EU has set an objective of reducing emissions by 80–95% by 2050. The existing 3R (Reduce, Recycle, Reuse) based on circular economy is insufficient for the aviation industry; the secret to Circular Aviation is 4R (Reduce, Recycle, Reuse, Redesign), which is only possible with improved aerodynamic designs for future aircraft/UAVs. The most significant aspect of 4R is "Redesign"; a highly improved design of aircraft is crucial for future zero-emission and climate neutrality goals. Therefore, aerodynamic improvements in the existing designs are the key to achieving this goal.

In order to achieve this goal, this study is specifically dedicated to investigations into the performance improvement of the 4R-UAV wing by implementing the PFCDs (Passive Flow Control Devices). Two types of PFCDs, i.e., MVGs (Micro Vortex Generators)

and winglets, were designed, optimized, and analyzed for final implementation on the 4R-UAV wing. The idea of such PFCDs is not new at all, and they have been successfully implemented for decades in large-scale aircraft; however, designing and implementing MVGs and winglets on a small-scale UAV with a wingspan of less than 2 m is not very common in nature, as information on PFCDs for low Re small-scale UAVs is limited. This limitation is further affected due to the requirement for decreased UAV weight and precise manufacturing (of small-scale MVGs with a height less than 1 mm). Additional challenges appear in designing, optimizing, integrating, and finally retrieving the enhanced performance for such small-scale UAV wings.

To understand the fundamental nature of the PFCDs, during recent decades, researchers have extensively investigated methods of optimization of UAVs using different wings, fuselage shapes, the application of passive flow control methods, etc. For instance, the bioinspired technique of leading-edge serrations has been investigated for different purposes experimentally and numerically. Wang and Zhuang [2] designed modified wind turbine blades with sinusoidal wave serrations applied on the leading edge to control the boundary layer separation in near-stall conditions. The numerical results of this study indicated that the leading-edge serration delayed the flow separation by employing the generation of the counter-rotating vortex pairs at a high angle of attack. In another study, Cai et al. [3] numerically investigated a modified airfoil with a single leading-edge protuberance at a low Reynolds number. Only one leading-edge serration was designed to isolate the serration geometry's impact on the wings' aerodynamic characteristics. The results showed that the stall angle of the modified airfoil was reduced compared to the original design. Furthermore, the pre-stall performance of the modified airfoil was decreased, whereas post-stall characteristics were enhanced. Moreover, Wei et al. [4] performed another experimental study that investigated the hydrodynamic characteristics of hydrofoils with leading-edge serrations at the Reynolds number of 1.4×10^4. The results of this study revealed that the effects of flow separation declined with the use of leading-edge serrations.

Another passive flow control method was designed by Kasper [5], which proposed the application of airfoils with a cavity. Theoretically, the principle of this concept was to create a convenient pressure gradient when two counter-rotating vortices inside the cavity are produced. These generated eddies over the suction surface can ensure an extra low-pressure region and cause a lower drag produced by the airfoil. This method has gained interest among aerodynamic researchers. Olsman and Colonius [6] investigated an airfoil with a cavity at a Reynolds number of 2×10^4. Their results revealed that the stall phenomenon was delayed utilizing counter-rotating separated flows, resulting in a reduced flow separation region. Still, aerodynamic efficiency (lift-to-drag ratio) throughout most AOA regimes was unclear in that study. A detailed numerical analysis regarding the aeroacoustics of NACA 0018 cavitied airfoil was reported by Lam and Leung [7] and Olsman [8] at Reynolds number 2×10^4. Cavitied airfoil produced less acoustic power, making it a less noisy airfoil design at low Reynolds number regimes compared to baseline designs. However, aerodynamic efficiency (C_L/C_D ratio) throughout most AOA regimes remains questionable.

Another approach to flow control is the application of the material surface roughness. The boundary layer flow gains momentum employing this passive flow control method, so the separated flow may be suppressed with re-energized flows, resulting in more stable flow characteristics without boundary layer separation [9]. The flow control method, by applying roughness material, is performed by intervening in the flow with the help of vortexes. Vortex sheds produced by roughness cause the flow in the boundary layer to gain more energy. Energized flow mixes with the boundary layer, thus suppressing flow separation and ensuring the flow moves along the airfoil surface. Vortex shedding can be used for different purposes over the surface of wings. For instance, the study conducted on the turbine blades of the gas turbine engine by Bai et al. [10] showed that the surface roughness could weaken the separation bubble of the turbine blade at a low Reynolds

number, thus reducing the aerodynamic loss while, at high Reynolds number, the surface roughness will trigger transient progress so that the losses can increase significantly.

VGs (Vortex Generators) are another type of passive flow control that provides stall delay by producing counter-rotating vortices that induce mixing of high and low momentum flows by transforming the laminar flow into turbulent flow in the near-wall regions [11]. VGs were employed in studies for reducing noise caused by flow separation, for reducing afterbody drag of fuselage and also for enhancing the performance of wind turbines. Many researchers have efficiently implemented Micro-Vortex Generators (MVGs). For example, Jirásek [12] and many others efficiently implemented Micro-Vortex Generators (MVGs) in UAVs for the flow control of the S-duct diffuser inlet section. Dol [13] enhanced the lift force of UAV from 160 N to 192 N and implemented VGs (at the leading edge of the wing) for lift improvement. These studies were good inspiration for implementing MVGs on the authors' small-scale 4R-UAV wings, even though they were implemented on medium or larger-scale UAVs. Based on this, the authors performed a short study [14] by implementing a limited number of MVGs on a small section of a UAV. Three types of MVGs (delta, rectangular, and trapezoidal) were designed and optimized for the small wing section at 19% chord location. The study was mainly conducted to see which type of MVGs are suitable for small-scale UAVs. With limited implementation, the trapezoidal MVGs performed relatively better than the other types. After the previous (preliminary) results, this paper extensively investigates the trapezoidal MVGs on the full wing of 4R-UAV, along with the winglets (as the two PFCDs).

NASA developed the concept of winglets in the 1970s, using multiple designs for different aircraft. Winglets are somewhat common for aircraft and have proven to improve the overall efficiency of large-scale wings for subsonic speed; however, implementing winglets on UAVs that commonly operate at low Reynolds numbers is extremely rare. Very limited work can be found in the literature and, especially. the winglets for small-scale UAVs are novel. R. Dagur [15] investigated the application of winglets on an operating UAV. A decrease in drag of 2.1% and 1.64% at 4° and 8° angles of attack was observed in the study. Similarly, Panagiotou [16] used blended winglets for MALE UAVs and found a significant rise in the UAV's aerodynamic performance and a 10% increase in endurance. Turanoğuz [17] studied the application of winglets on a large-scale tactical UAV with a payload of 60 kg and a wingspan of 10 m. The investigations were conducted on three wing configurations (one baseline wing and two wings with winglets). As the investigations were performed on the large-scale UAV, the best-performing winglets exhibited improvement of up to 8% in C_L/C_D ratio, compared to the baseline design. These studies are good motivation, but as mentioned earlier, for small-scale UAVs, it is always a concern, due to the very small wingspan range of 0.5–2 m and operation at lower altitudes and speeds. Metrinho [18] designed a variable-span morphing wing for a small-scale UAV and performed experiments for performance evaluation. At the cruising speed, the drag force was reduced by 20% compared to that of fixed-wing aircraft. The morphed wing is not exactly a winglet, but the study showed that the wing geometry alteration might deeply impact the performance.

In this study, a stepwise approach was adopted to investigate the feasibility of the PFCDs on the small-scale 4R-UAV's wing. The baseline wing was designed with the authors' SG6043mod airfoil, which was optimized for low Re range and enhanced aerodynamically. PFCDs (MVGs and winglets) were investigated in the next step by implementing them on the baseline wing. Finally, the overall impact of the PFCDs on the baseline wings was analyzed to understand the feasibility of their implementation in small-scale UAVs. The study found that both the PFCDs provided their respective benefits. For example, MVGs enhanced the wing's near-stall properties and delayed the stall by up to 2°, while the wing's maximum lift was increased up to 6% mainly at later angles of attack. Winglets, on the other hand, were especially useful at the lower angles of attack and enhanced pre-stall properties by decreasing the induced drag and improving the aerodynamic performance by more than 8%. Both the MVGs and winglets, when installed on the 4R-UAV wing, enhanced the

overall aerodynamic performance at all angles of attack. In summary, the study successfully implements PFCDs on the small-scale UAV (4R-UAV) wing and recommends their use, together or separately, based on the mission requirements.

2. Investigation Methodology

For a smooth workflow, this computational study was performed in defined steps. In the first step, the baseline wing was designed after a series of aerodynamic and geometric calculations (based on the future 4R-UAV variants). Based on the authors' previous study [19] conducted for the aerodynamic improvement of the UAV wings, the wing of the small-scale 4R-UAV (in this study) was designed from the aerodynamically optimized airfoil. In the next step, the implementation of the Passive Flow Control Devices (PFCD) was carried out in two sub-steps: (i) Micro Vortex Generators (MVGs) and (ii) winglets. A short study on the MVGs on a wing segment was conducted by [14] and, based on this, the implementation of MVGs was investigated for the performance analysis of the full-scale wing of the 4R-UAV. For the winglet(s) investigations, a detailed analysis was performed to design and optimize winglets suitable for the small-scale UAV class. In the final step, aerodynamic performance analysis was carried out for the full-scale 4R-UAV with integrated MVGs and (the most appropriate) winglets. Figure 1 illustrates the workflow diagram of the implementation steps.

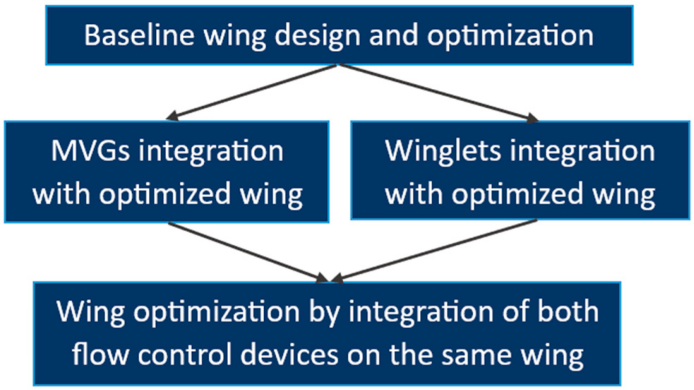

Figure 1. UAV PFCD implementation workflow.

For the 4R-UAV wing design, the SG6043mod airfoil was chosen for its proven aerodynamic capabilities. This airfoil was developed by [19] and was aerodynamically optimized for low Re and small-scale applications. The SG6043mod airfoil provides an enhanced lift-to-drag ratio as this is vital for the performance and endurance of the aircraft. A detailed comparison between the ordinary wing designed from the SG6043 and the optimized SG6043mod airfoil has already been studied by [19], where the optimized wing manifested enhanced aerodynamic performance (compared to that of the parent wing). The original SG6043 airfoil (developed by Selig and Giguere [20]) possesses several qualities that are advantageous in terms of endurance, which is a primary concern of today's electrically powered UAVs. On the other hand, the SG6043mod is the optimized airfoil providing improved aerodynamic characteristics for the low Reynolds number range of 3×10^5 [19]. 4R-UAV, which is a small-scale UAV, is designed to operate in the Re range of 2.5×10^5–3×10^5. Based on these advantages of SG6043mod airfoil, the baseline wing was designed from this airfoil. Figure 2 shows the enhanced drag polar of the optimized airfoil (SG6043mod) compared to the original airfoil (SG6043). In summary, the first stage of the aerodynamic improvement for the 4R-UAV was already attained at the wing design stage.

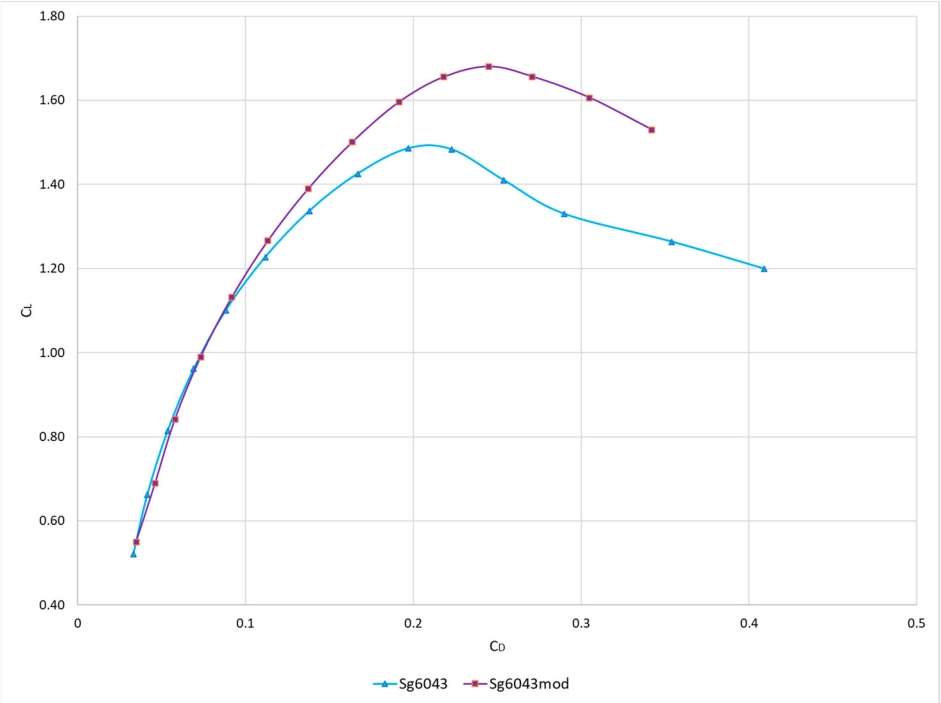

Figure 2. Comparison of drag polar of the original airfoil (SG6043) and optimized airfoil (SG6043mod).

As 4R-UAV is not designed for a specific mission, the main goal is to design a multipurpose small-scale UAV for a range of civilian and defense applications. For the wing design parameters, Xiong [21] suggested the relationship between the wingspan range and the maximum takeoff weight. Based on Xiong's [21] work, a range of 4–6 kg maximum takeoff weight and 1.5–2.0 m wingspan were selected as the initial design parameters of the 4R-UAV.

The weight to wingspan ratio is given in Equation (1):

$$W_{TO} = 1.5313b^{2.2045}, \quad (1)$$

where:

W_{TO}—take-off weight.

$$b \text{ (wingspan)} = (W_{TO}/1.5313)^{0.4536},$$

For the maximum takeoff weight of 6 kg, the calculated value (from Equation (1)) for the wingspan of the 4R-UAV was 1.86 m.

In the next step, wing surface area and lift force were evaluated. For the wing surface area, [22] and other studies [13,21–23] suggested an iterative approach for the selection of cruising angle of attack and surface area. For this, the authors' previous study [19] was found to be useful, which provided an initial approximation for the wing area and expected values of C_L. Figure 3 illustrates the C_L variations with angle of attack for the wing designed from SG6043mod airfoil for light aircraft applications. Usually, a hit and trial-based iterative analysis is relied on for the cruising angle and surface area calculations. Therefore, after the initial iterative analysis, a CFD analysis of the initial wing segment was carried out. Figure 4 shows the plot of the aerodynamic efficiency against the angle of attack, where the maximum efficiency can be observed at 4° angle of attack. Based on this, the 4° angle was chosen as the cruising angle of the 4R-UAV. The surface area of the wing was calculated at the 4° cruising angle from the lift equation:

$$L = C_L \times r \times V^2 \times S/2, \quad (2)$$

where: L—lift;
C_L—lift coefficient;
r—air density;
V—freestream velocity;
S—wing area.

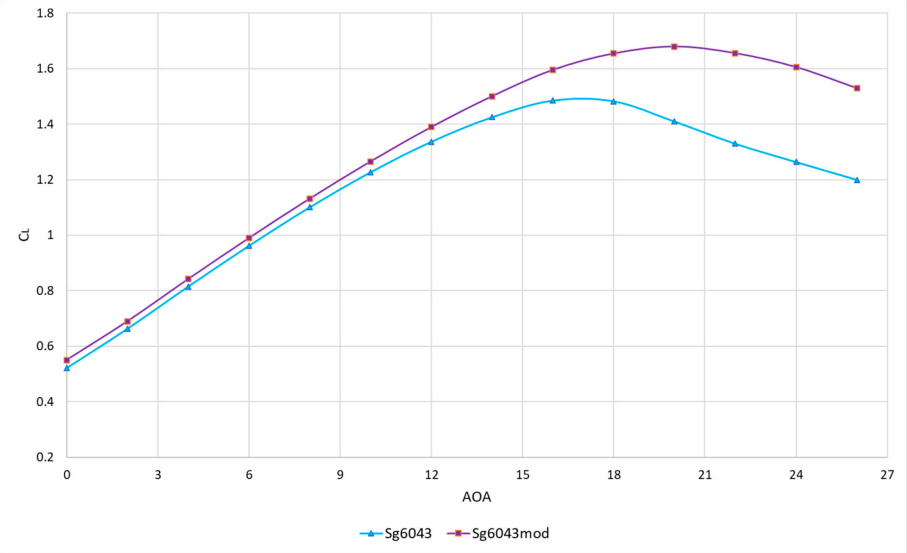

Figure 3. Relation between lift coefficient and angle of attack of SG6043mod.

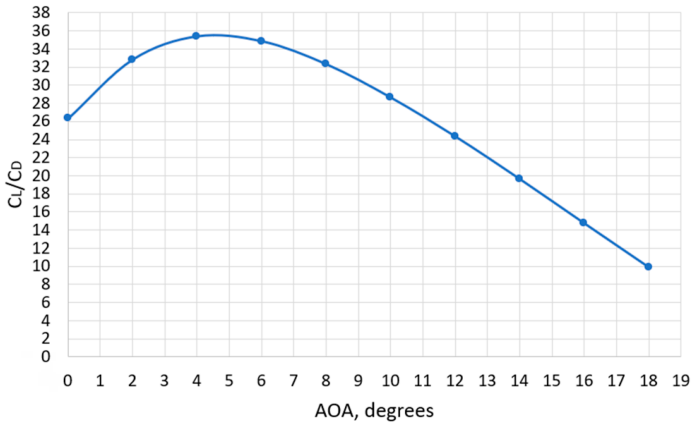

Figure 4. Lift-to-drag ratio of the baseline wing segment vs. AOA.

The calculated wing surface area was 0.289 m^2 at the planned cruise speed of 20 m/s, while the minimum chord length was calculated as 0.1558 m. In order to reduce the required angle of attack or flight speed, a safe chord length and surface area were chosen as 0.18 m and 0.334 m^2, respectively, for the final wing. Table 1 summarizes the design parameters of the UAV baseline wing, while the 3D CAD model of the baseline wing is illustrated in Figure 5.

Table 1. Design parameters of the UAV wing.

MTOW, kg	b, m	Cruise AOA, °	C_L Cruise	S, m^2	c, m	V, m/s
6	1.858	4	0.83	0.334	0.18	20

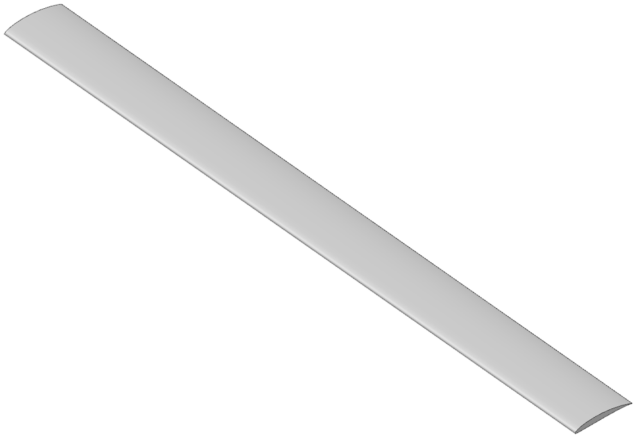

Figure 5. Baseline wing design.

3. Investigation of Passive Flow Control Devices

As planned, the implementation of the Passive Flow Control devices on the designed wing was investigated using two devices: (i) Micro Vortex Generators (MVGs) and (ii) Winglets.

3.1. Micro-Vortex Generators (MVGs): Parameter Calulation and Design

Mueller-Vahl et al. [24] explained that MVGs installed at 15–20% chord length from the airfoil's leading edge are ideal for realizing the stall delay and increasing the maximum lift coefficient. Brief and early-level study [14] of MVG implementation on the low-speed wing segment was performed by the authors, which provided an initial understanding for further implementation of the MVGs on a full-scale wing of the 4R-UAV (in this study). For the small wing segment [14], only trapezoidal-type MVGs provided a good agreement in terms of aerodynamic characteristics. In addition, authors found that 19% chord length was the most suitable location for the MVGs on the wing, provided that they are installed at a specific angle of 18° relative to the flow. The design details, computational scheme, and the results of comparison of different types of MVGs can be found in the authors' previous study [14], while the investigations for the implementation of trapezoidal MVGs on the full-scale wing is presented in the later section of this paper (together with the winglets). The final geometric parameters of the trapezoidal MVGs (to be implemented on the 4R-UAV wing) are presented in Table 2, while the design of the trapezoidal MVGs and their installation strategy is indicated in Figure 6.

Table 2. Trapezoidal MVGs geometric parameters.

H1, mm	H2, mm	W, mm	L, mm	A, mm
0.6	0.95	0.6	3.5	6

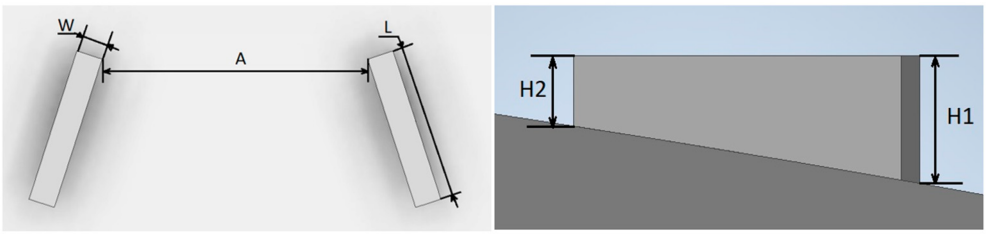

Figure 6. Installation strategy of the trapezoidal MVGs illustrating 18° installation angle to the flow (top and side views).

For the MVG designs, three types, i.e., delta, rectangular, and trapezoidal MVGs, were investigated. All MVG configurations offered delayed wing stall. The stall angle for the baseline wing segment was 14° while the stall angle for delta, rectangular, and trapezoidal MVGs were 15°, 16°, and 16°, respectively. Trapezoidal MVGs also exhibited the maximum lift coefficient (C_L), which was more than 5% compared to the baseline wing. Considering the aerodynamic efficiency of the wing, all MVGs showed a drop in the early angles of attack, with the exception that the trapezoidal MVGs manifested an insignificant drop in the early angles of attack. Moreover, a sharp increase in aerodynamic efficiency was observed in trapezoidal MVGs at later angles of attack (near stall region), as shown in Figure 7.

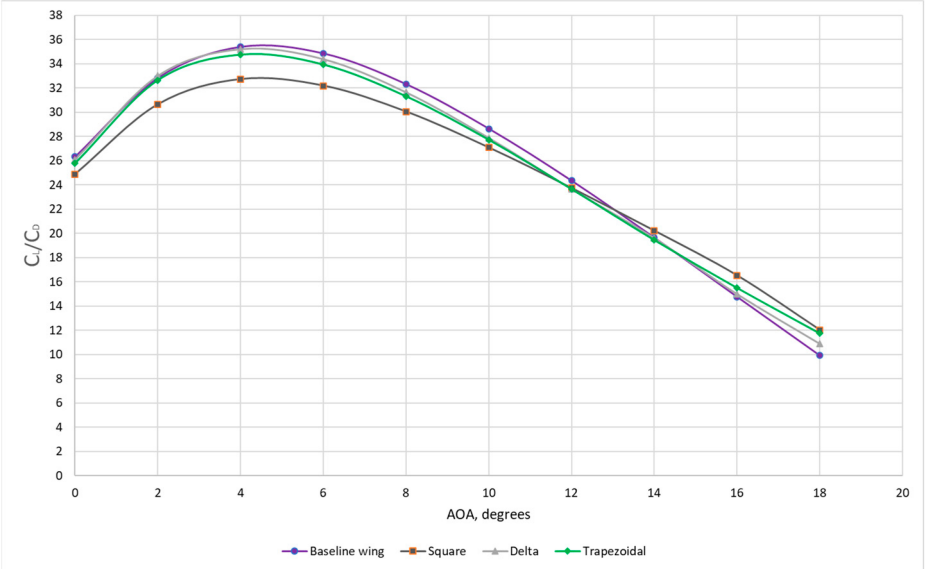

Figure 7. Comparison of aerodynamic efficiency between baseline wing and MVGs.

Trapezoidal MVGs offered improved aerodynamic characteristics, especially in terms of significantly delayed stall. However, the improvement was only limited to a higher angles of attack, which led authors to implement another type of passive flow control devices, i.e., winglets, in order to harness the maximum possible aerodynamic efficiency at the lower angles of attack. The idea of implementing winglets on such a small-scale UAV wing is very challenging and novel in the sense that a successful implementation of winglets may open new research direction in small-scale UAVs wing designs. The details of the winglet(s) design and implementation are explained in the following section.

3.1.1. Winglets: Design, Investigation, and Implementation

Winglets were the second type of Passive Flow Control Devices (after MVGs) investigated for the performance enhancement of the 4R-UAV wing. As mentioned, the target was to achieve improved performance at the earlier angles of attack (after MVGs contributed to stall delay and improvement at the later angles of attack). Winglets are extremely common structures in commercial aircraft wings, contributing to reducing induced drag. NASA pioneered the winglets in the mid-70s and, since then, several designs have been implemented. On the contrary, the idea of implementing winglets on small-scale UAVs is somewhat neglected due to low speeds and limited wingspans [25,26]. Due to the small-scale and mainly low-speed applications, the benefits of winglets on UAVs are limited to non-existent. However, from the research point of view, the design and performance analysis of the PCFDs, especially winglets, possess an enormous potential, which should be addressed in-depth in the scientific literature. Limited but outstanding studies were performed on UAV winglets. For example, Panagiotou [16] and Dagur [15] studied the impact of winglets on UAVs, including Medium-Altitude-Long-Range-Endurance (MALE) UAVs and were

able to marginally reduce the drag or increase endurance. Unfortunately, these studies were performed on large-scale UAV wings only, but in small-scale UAVs with wingspans of 0.5–2 m, such marginal rise in performance may fade.

Based on the above factors, there were three main challenges regarding the winglet implementation: (i) to design the most appropriate winglet configuration for the designed small-scale (short-span) 4R-UAV wing, (ii) to improve the aerodynamic performance of the 4R-UAV at the lower angles of attack, (iii) finally, integration of the winglets along with the MVGs on the 4R-UAV wing to achieve the overall aerodynamic benefits at all AOA regimes (lower to higher angles of attack).

For the initial design stage of winglets, no standard method can be devised, since flow characteristics highly depend on the wing geometry and flight environment. The only useful way is to design several configurations of the winglets (based on the wing geometry and flight conditions) and analyze them computationally. For this, the authors developed six completely new winglet configurations for 4R-UAV wings. These configurations were designed based on wing geometry and flight conditions. Four main design parameters were considered for the winglet configurations, i.e., (i) winglet span (distance from winglet root to winglet outer edge), (ii) winglet height (distance between winglet root and tip), (iii) cant angle (angle between the horizontal plane and winglet), (iv) winglet root to tip chord ratio. Table 3 illustrates the geometric parameters of the six winglet configurations, while these configurations are shown in Figures 8–13. The first three winglet configurations are the commonly used blended winglets. The 4th configuration is the blended winglet configuration with a larger arc radius. The 5th configuration is the wingtip fence winglet type. The last 6th configuration is the blended winglet with an additional flow divider with a 30° tip vertex and two 60° base vertices. All six winglet configurations were designed based on the cant angle range of 50–90 degrees, as prescribed by Panagiotou's study [16].

Table 3. Winglets' geometrical parameters.

Winglet Configuration	Winglet Type	Span, mm	Height, mm	Cant Angle, °	Root to Tip Ratio
No. 1	Blended	34	58	90	3.3
No. 2	Blended	67	70	50	3.3
No. 3	Blended	50	109	75	3.3
No. 4	Blended	122	122	75	7.4
No. 5	Wingtip fence	N.A	130	90	3.3
No. 6	Blended (with flow divider)	122	122	75	7.4

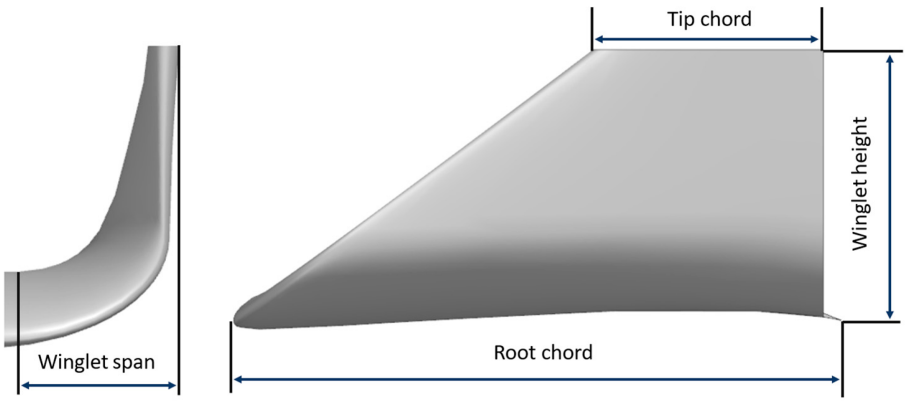

Figure 8. Winglet configuration No. 1, front view, and side view.

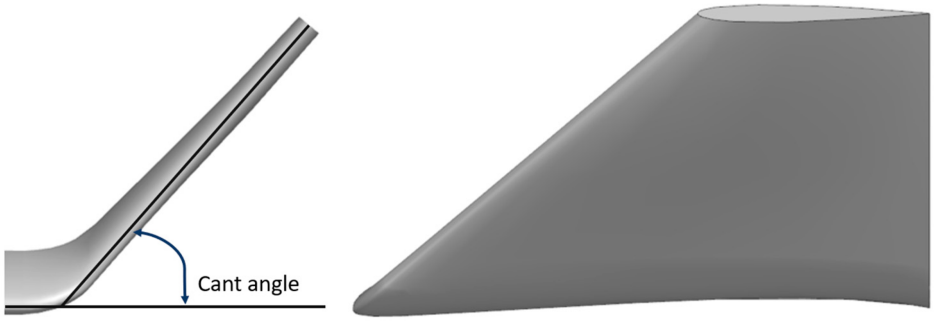

Figure 9. Winglet configuration No. 2, front view, and side view.

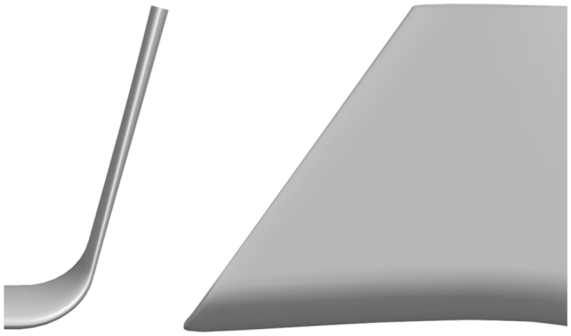

Figure 10. Winglet configuration No. 3, front view, and side view.

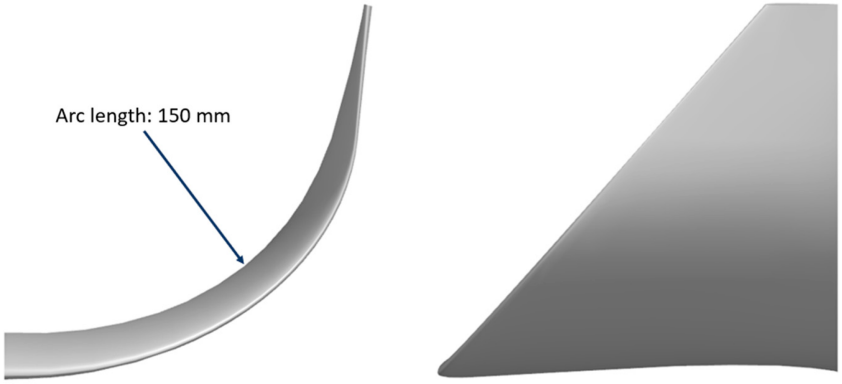

Figure 11. Winglet configuration No. 4, front view, and side view.

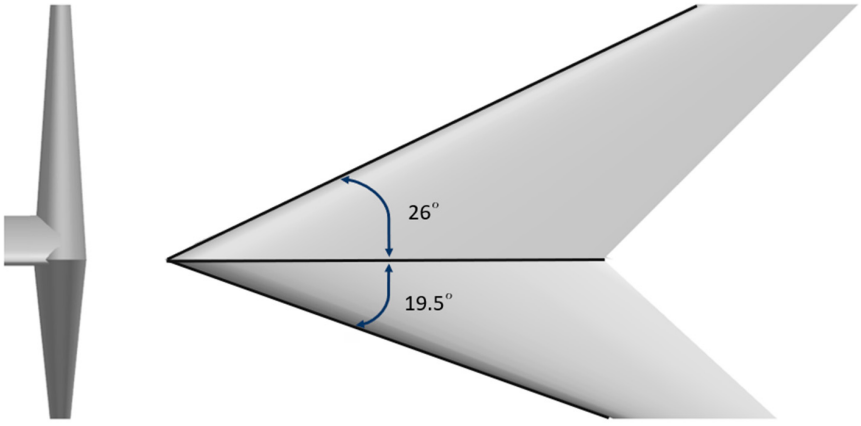

Figure 12. Winglet configuration No. 5, front view, and side view.

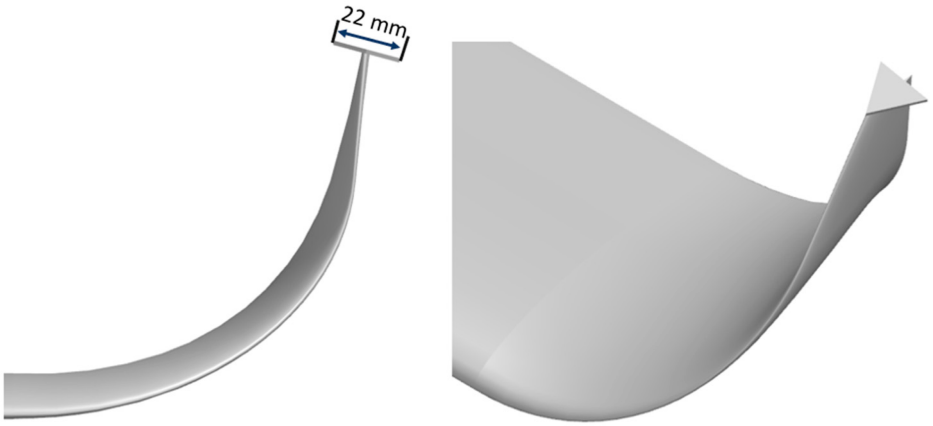

Figure 13. Winglet configuration No. 6 (blended winglet of configuration No. 4 with installed "flow divider" on the tip).

3.1.2. Winglets: Computational Scheme

This subsection briefly describes the control volume domain and mesh generation for winglet analysis. For the winglets' designs, the control volume was chosen as 1.4 m (8 chord lengths) in height, 2.5 m (14 times the chord length) in length, and 3 m (17 times the chord lengths) in width to ensure accurate and precise analysis. In order to save computational resources and time, the half-span wing was used for grid generation. For winglet geometry, about 10 million elements of mesh were used. Figure 14 shows the adopted grid scheme for the computational comparison of different winglet configurations. Mesh was optimized according to each winglet configuration; Figure 15 illustrates the surface mesh of the winglet configuration 4, where mesh density can be observed.

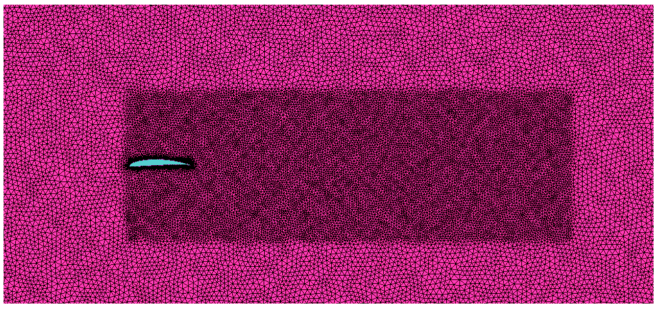

Figure 14. Mesh elements' density variation in the control volume.

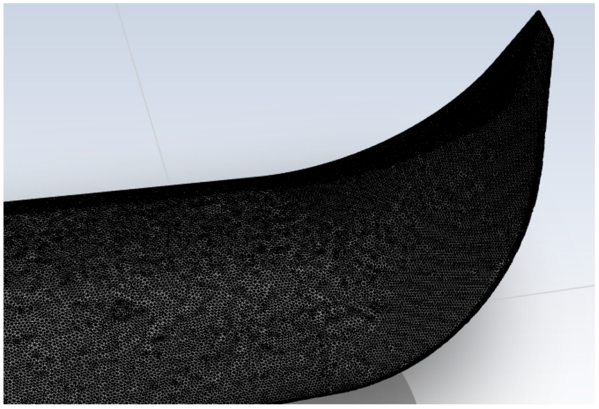

Figure 15. Winglet surface meshing.

In order to observe the impact of the control volume size on the results, an additional "domain independence study" was performed to ensure that the results' precision would not suffer from the domain size adopted for this study. For this, a larger control volume was created with a height of 40 times the wingspan, length of 70 times the wingspan, and width of 20 times the wingspan. The element counts for this enlarged mesh reached 40 million mesh elements (15 million more elements than the adopted mesh to ensure that mesh density is high enough to capture flow characteristics properly even at far distance from the wing). Figure 16 illustrates the comparison of the size between the adopted (in white) and enlarged (in black) mesh control volumes (for the domain independence study). The adopted control volume (inside the enlarged control volume of Figure 16) sustained the original mesh density and element distribution, because the enlarged control volume was created around the adopted volume by extending its initial parameters. This enlarged control volume was analyzed at 0° angle of attack. The results of this domain independence study manifest that the impact of control volume size is nearly negligible (less than 2% difference in C_L, C_D, and C_L/C_D). Therefore, the adopted (smaller) control volume was chosen for all simulations of the PFCDs. The summary of the difference in results in three main parameters (C_D, C_L and C_L/C_D ratio) for 0° AOA is summarized in Table 4 (for final wing design).

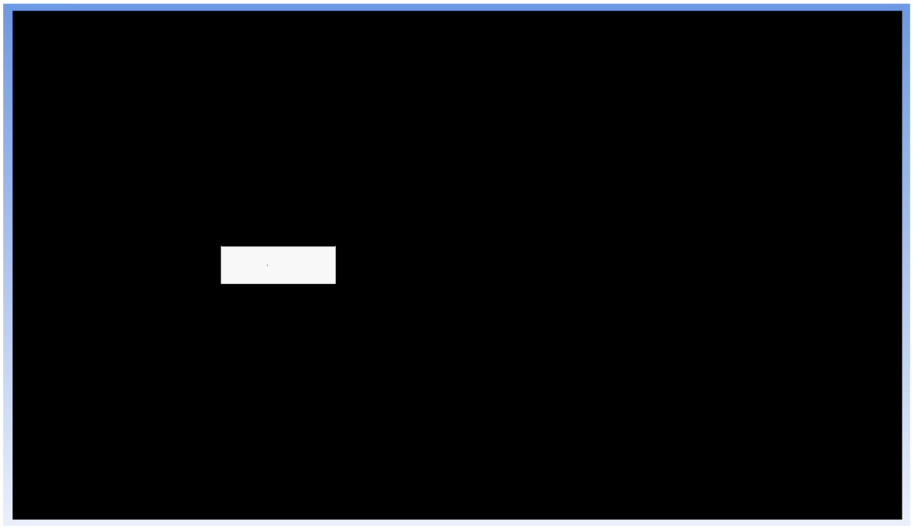

Figure 16. Domain sizes' comparison of the adopted (white) and enlarged (black) control volume for domain independence study.

Table 4. Results of domain independence study.

Adopted Domain			**Enlarged Domain**			**Difference (Relatively to Adopted Domain), %**		
C_L	C_D	C_L/C_D	C_L	C_D	C_L/C_D	C_L	C_D	C_L/C_D
0.5569	0.02226	25.015	0.5549	0.02182	25.433	−0.34	−1.98	1.67

For the computational setup, a freestream velocity of 20 m/sec was used as the inlet boundary condition, standard 1.225 kg/m^3 was taken as air density, while standard atmospheric temperature and pressure were used for the simulations. The calculated Re for the computational scheme was 3×10^5. k-ε RNG turbulence model was implemented to accurately capture the winglets' vortex flow.

3.1.3. Winglets' Aerodynamic Performance Comparison

For the aerodynamic performance, the results of all the winglet configurations were compared. Winglets' efficiency was mainly analyzed using the same parameter as for

the MVGs (Figure 7), aerodynamic efficiency of the wing (C_L/C_D ratio). The winglets' aerodynamic performance is compared here:

Coefficient of drag: The primary purpose of winglets in aircraft is to reduce the induced drag by weakening the tip vortex. Therefore, it is logical to compare the drag coefficient first. Figure 17 illustrates the comparison of all winglet configurations with respect to the baseline wing (the two lower parts of Figure 17 are illustrating zoomed in regions of 4 to 12 and 12 to 18 degrees AOA for better readability of the results). All configurations slightly (up to 10%) reduced the drag coefficient compared to the baseline wing. For now, it is safe to say that none of the configurations contribute to enhanced drag. However, winglet configuration 4 is slightly better in terms of drag reduction. Positively, the drag trend of all the configurations is continuous in all the AOA regimes, and it only starts to rise after the wing stall (14° AOA).

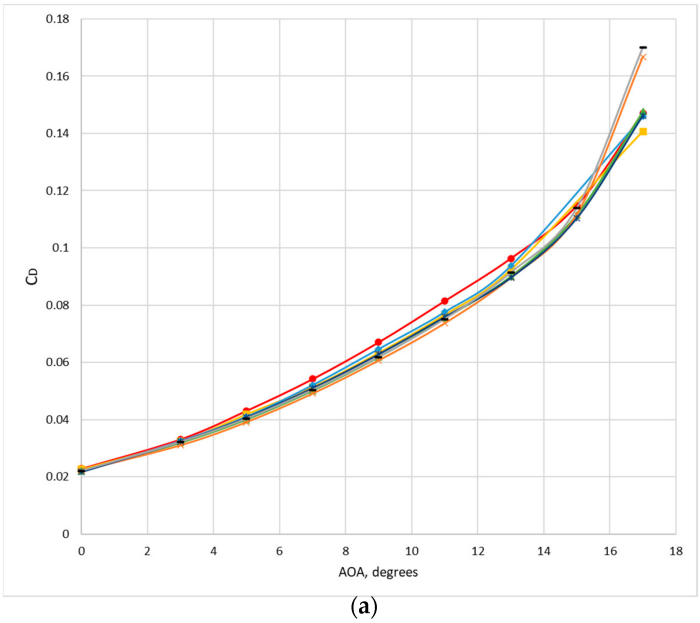

(**a**)

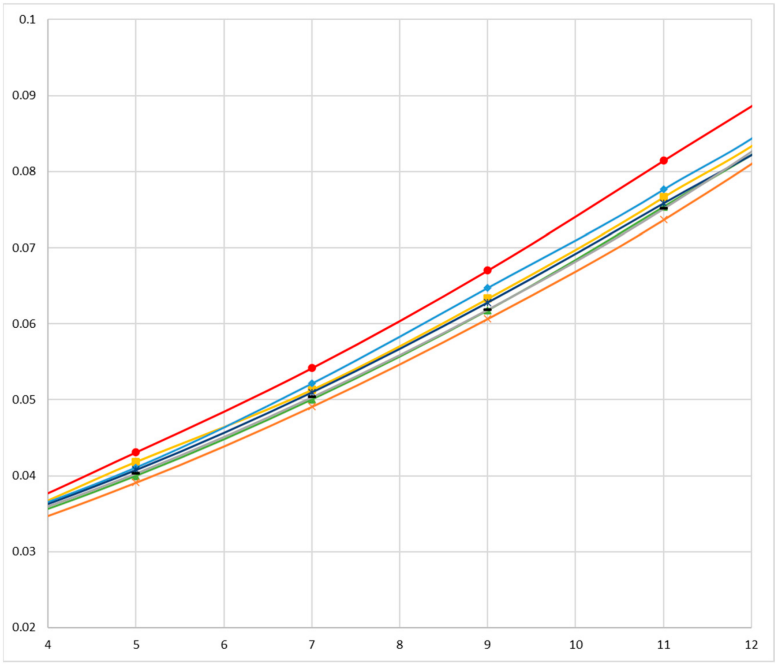

(**b**)

Figure 17. *Cont.*

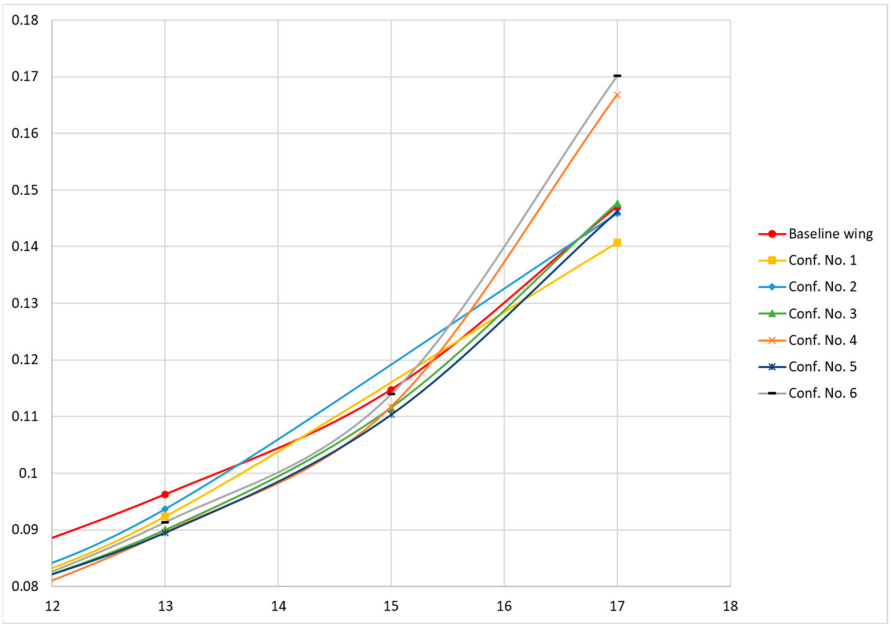

(**c**)

Figure 17. C_D Vs. AOA graph of the baseline wing and different winglet configurations; (**a**) shows overall trends, while (**b**,**c**) show their respective AOA regions (4–12° and 12–17°) for better reader perception.

Aerodynamic efficiency: Aerodynamic efficiency (C_L/C_D vs. AOA) is the most significant parameter with which to assess the aerodynamic performance. The aerodynamic efficiency of all six winglet configurations is compared with the baseline wing in Figure 18 (the two lower parts of Figure 18 are illustrating zoomed in regions of 0 to 9 and 9 to 18 degrees AOA for better readability of the results). The main objective of implementing the winglets on the UAV wing was to gain the aerodynamic advantage at lower angles of attack, as MVGs enhanced the performance only at higher angles of attack, in addition to the delayed stall. Configuration 4 and 6 improved performances relatively better than all other configurations. The decrease in performance is only after the stall angle (14°), which is irrelevant.

From the comparison plot (Figure 18), from this graph it is quite difficult to understand which exact winglet configuration is the best-performing one; for this, non-dimensional percentage increment relation in Equation (3) was used:

$$\text{Aerodynamic efficiency increasement} = ((C_{LW}/C_{DW})/(C_L/C_D) - 1) \times 100\%, \quad (3)$$

where:

C_{LW}—lift coefficient of the winglet configuration

C_{DW}—drag coefficient of the winglet configuration.

C_L—lift coefficient of the baseline wing design

C_D—drag coefficient of the baseline wing design.

The results retrieved after applying Equation (3) are demonstrated in Figure 19. For the assessment of the performance improvement, the baseline wing's performance was taken as the standard; hence, it was considered as the baseline of performance improvement (placed at the origin as the horizontal axis). The improvement in performance (percentage increment) is highest in the winglet configuration 4 across all AOA regimes. Interestingly, in configuration 6, the flow divider (installed on the winglet of configuration 4) did not provide any significant performance improvement compared to configuration 4. The flow divider was installed to further weaken the wingtip vortex strength; however, this was in vain. At the 4° angle of attack (the cruise angle of the 4R-UAV), the performance improvement of the configuration 4 was 6%, and the maximum performance improvement of nearly 8.5% was observed at 8° angle of attack.

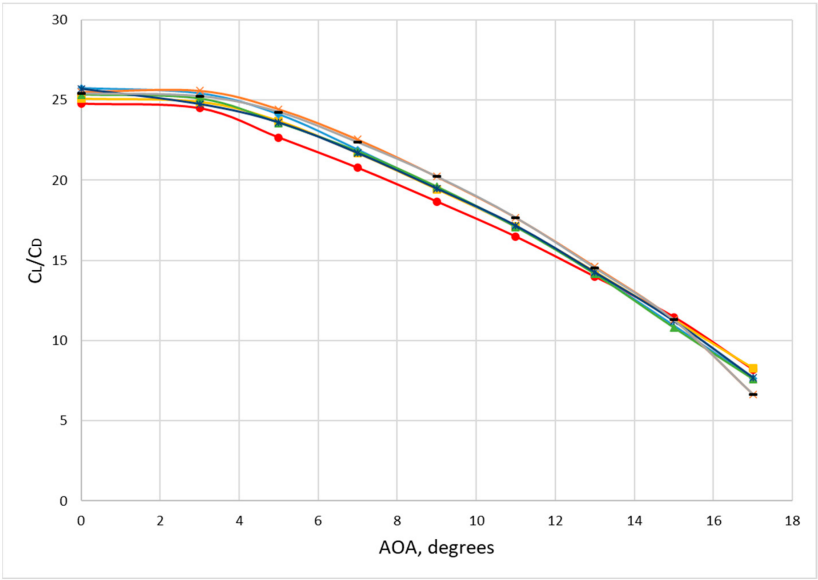

(**a**)

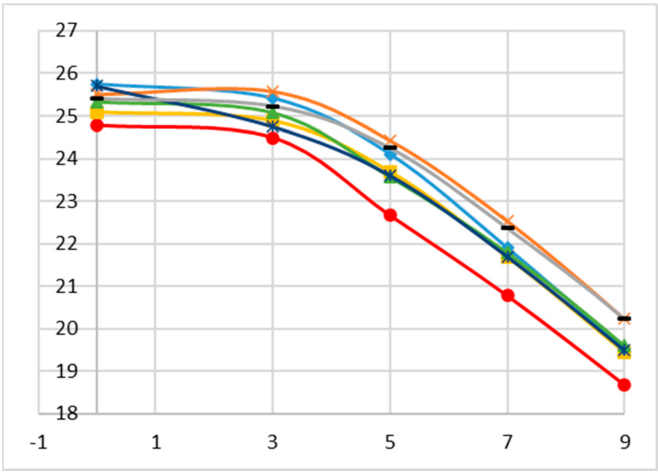

(**b**)

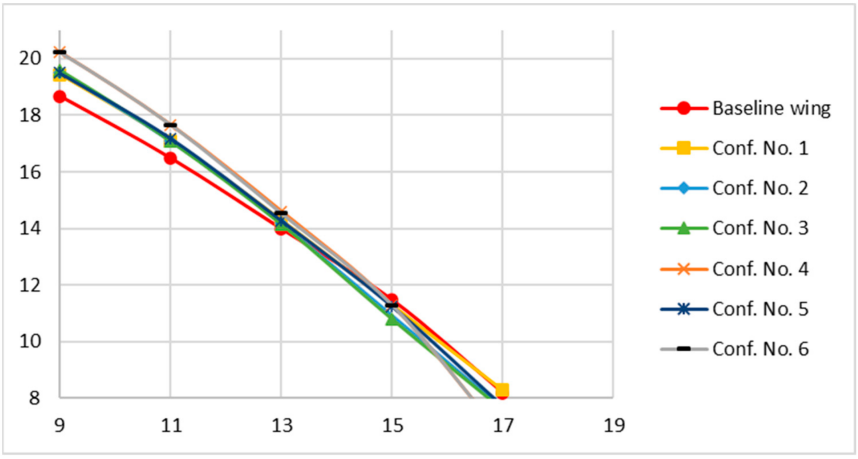

(**c**)

Figure 18. Lift-to-drag ratio Vs. AOA graph of the baseline wing and different winglet configurations; (**a**) shows overall trends, while (**b**,**c**) show their respective AOA regions (1–9° and 9–17°) for better reader perception.

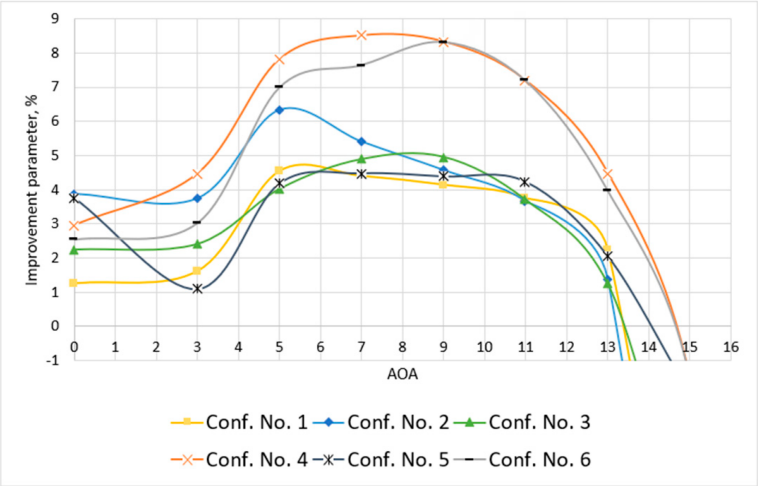

Figure 19. Lift-to-drag ratio enhancement vs. AOA.

After this comparative winglet analysis, blended winglets configuration 4 was chosen for the final implementation on the 4R-UAV wing. The difference between the configurations is marginal; however, configuration 4 manifested the most improved results. Therefore, from here on in this paper, winglet configuration 4 will be simply referred to as 'winglet' and only these results will be considered for the analysis.

3.1.4. Winglet Flow Mechanism

Based on the performance comparison, the selected winglet flow mechanism was compared with the baseline wing. Figure 20 depicts the deviation in surface streamlines originating from the baseline wing tip and the winglet. The core of the tip vortex from the winglet is slightly shifted towards the winglet tip. The vortex core in the wing is at the tip while, in the winglet case, the vortex core is at the arc center of the winglet. Figure 21 illustrates a clearer view of the flow over the respective wings' surfaces at a 100 mm downstream station wing's trailing edge. The tip vortex generated a flow breakdown and prolonged vortex, as observed in Figure 21a. On the other hand, the winglets decreased pressure coefficient gradient between suction and pressure sides of the wing, which helped keep the flow attached to the surface smoothly, as seen in Figure 21b. The smooth flow over the winglet surface seems to be the reason for the enhanced performance.

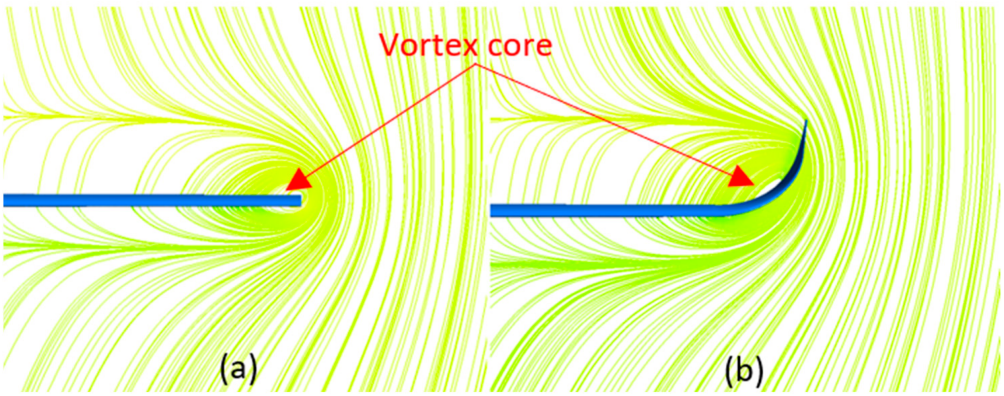

Figure 20. Tip vortex flow mechanism at a 100 mm downstream station wing's trailing edge: (**a**) baseline wing; (**b**) winglet.

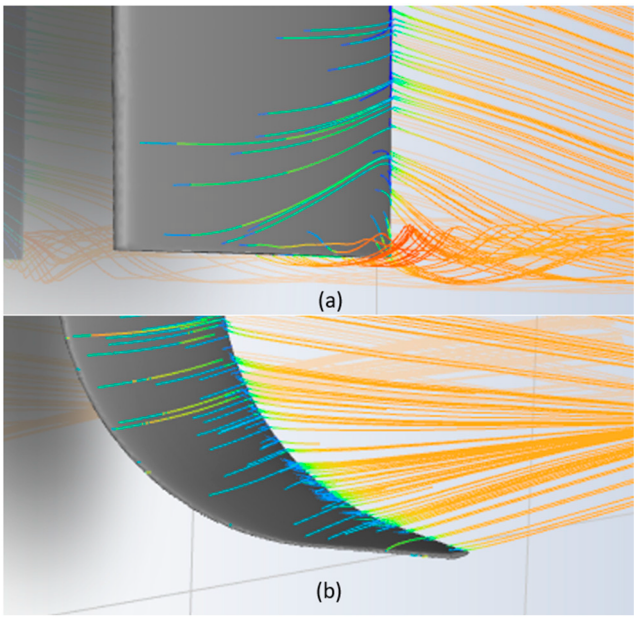

Figure 21. 3D streamlines of the vortex flow: (**a**) baseline wing (**b**) winglet.

Pressure distribution contours over the suction sides of the baseline wing and winglets are shown in Figure 22. Pressure distribution near the wingtip of winglets is more even compared to the baseline wing. Winglets offered higher pressure at the tip region compared to the baseline wing, which led to lower pressure gradients between suction and pressure sides where the vortex is less intensive. Baseline wing pressure drops due to a strong vortex and its localized features closer to the wingtip trailing edge results in a slightly higher lift coefficient than for winglets but, at the same time, the drag coefficient had also decreased, with an exceeded rate than that of the lift.

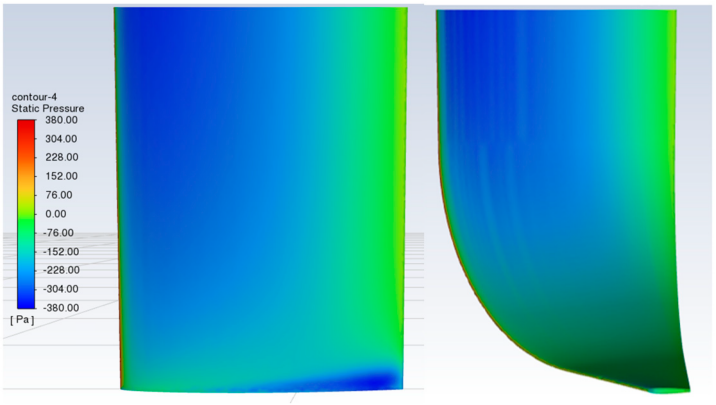

Figure 22. Pressure distribution over suction side of the (**a**) baseline wing and (**b**) winglet.

The winglet's main purpose is to reduce the drag, which can be correlated with the shear stress distribution on the wing surface, as shown in Figure 23. The wing with winglets installed experienced lower shear stress over the whole wingtip region of the wing compared to the baseline wing. The wingtip vortex produced in the wingtip regions caused an increased velocity gradient in that region, which further increased the shear stress at the wingtip trailing edge. On the other hand, the vortex produced in winglets had less strength due to the geometry of the winglet, which delayed the attachment of the vortex with the wing surface and, hence, reduced drag.

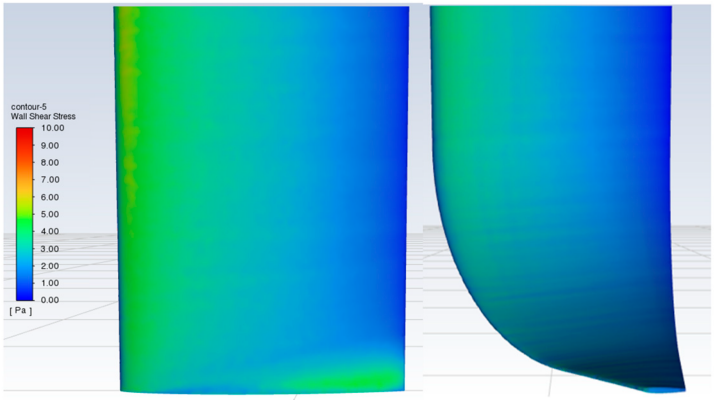

(**a**) (**b**)

Figure 23. Shear stress distribution over suction side of (**a**) baseline wing and (**b**) winglet.

Overall, winglets improved the performance, especially at the lower angles of attack. In the final section, the application of both the PFCDs will be investigated.

3.1.5. Final Wing Design

For the final wing design, the main task was to implement both the PFCDs on the baseline wing. The most efficient MVGs, i.e., trapezoidal type MVGs, were installed at 19% (proven as the most appropriate location) of the chord [14]. In addition, winglets (configuration 4) were also installed on the baseline wing along with the MVGs for the final computational analysis. Figure 24 illustrates the semi-span of the UAV final wing 3D model with integrated PFCDs.

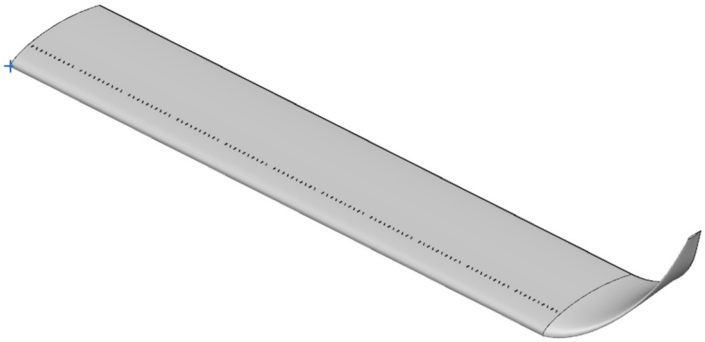

Figure 24. UAV final wing design with integrated winglet and MVGs.

3.1.6. Final Wing Design: Computational Scheme

For the computational analysis, the grid scheme for the final wing design was similar to the one developed for the winglets' investigation. The main task was to accommodate the mesh for the installed MVGs. For this, mesh density was significantly increased near the MVG regions, due to which the number of elements had to be increased from 10 M to 25 M. Figure 25 depicts the surface meshing of the wing. Due to the extremely dense mesh and small size of MVGs, capturing the mesh around MVGs precisely was difficult without losing the figure quality. The zoomed-in view of the grid strategy around the MVGs is given in Figure 26.

A mesh independence study was performed to ensure that the mesh variations have no impact on the results and are acquired precisely and accurately. Four different mesh strategies were created based on the number of elements. Figure 27 illustrates the mesh independence chart where the value of the lift force remains nearly constant (the maximum variation of results between heaviest and lightest meshes was less than 3%) after the 25 M

grid elements, and the mesh does not impact lift variations; therefore, 25 M mesh elements were used for the analysis for the sake of minimal computational cost.

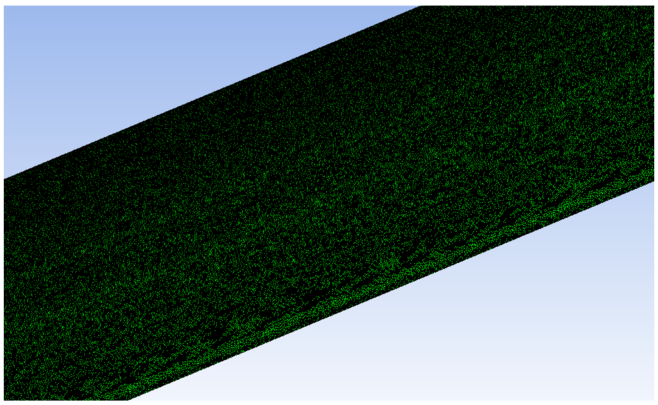

Figure 25. Wing surface mesh strategy.

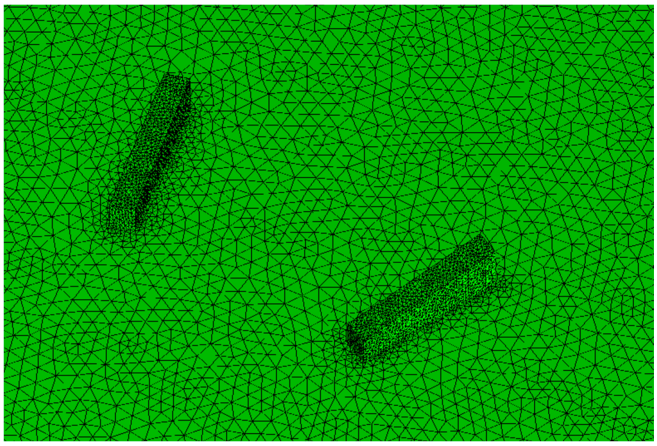

Figure 26. Close-up view of the mesh scheme near the MVG region.

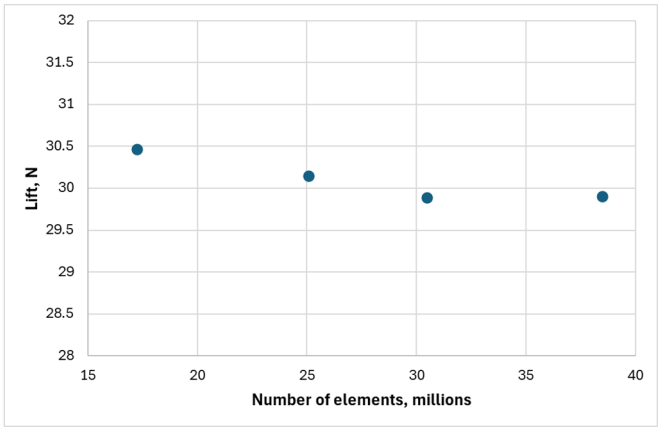

Figure 27. Mesh independence trend for the study.

The numerical scheme was kept the same for the final wing design, as used for winglet analysis. For the final wing design, which includes winglets as well as extremely small MVGs, the k-ε RNG turbulence model was employed due to its better capabilities for near wall boundary layer treatment and to account for the effects of smaller scales of motion.

3.1.7. Final Wing Design: Investigation Results

The performance of the final wing, which was integrated with the winglet and MVGs, was compared with the baseline wing. The two passive flow control devices were implemented to get the maximum aerodynamic advantage at all angles of attack (0° to stall angle). The MVGs were good for later angles of attack, while the winglets were advantageous at early angles. The main aim was to see if both PFCDs provide benefits or suppress one another's performance enhancements. For this, a step-by-step comparison was drawn and explained here.

Coefficient of lift (C_L) and drag (C_D): The comparison of the lift and drag coefficients between the baseline and final wing is shown in Figures 28 and 29, respectively. In the final wing, the lift coefficient increment can be observed in the later angles of attack, mainly coming from the MVGs. Importantly, compared to the baseline wing, in the final wing, the stall angle of the final wing was delayed by 2° (13° to 15°), while the maximum lift coefficient was increased to nearly 6%. On the other hand, the main purpose of the winglets in aircraft is to reduce the induced drag, which was also observed in this study where configuration 4 winglets provided a slightly better advantage (up to 6% reduction in drag coefficient). After the inclusion of the MVGs (in the final wing design), the drag effect was unchanged, as seen in Figure 29. In a way, the winglets compensated for the additional drag produced by the MVGs at the lower angles of attack [14].

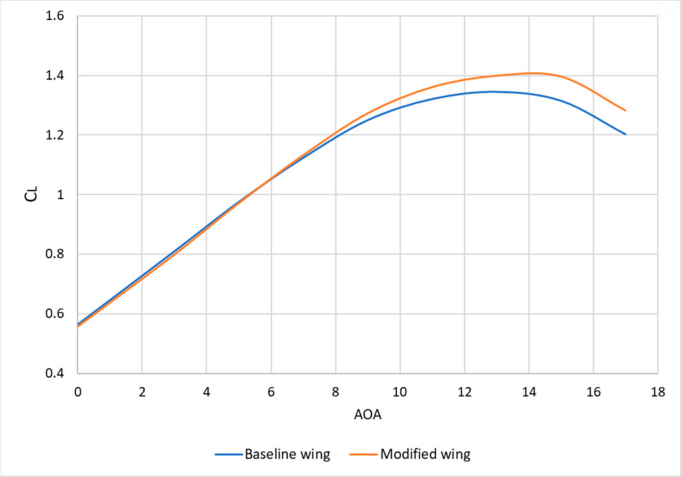

Figure 28. Comparison of the baseline and final wing lift coefficient trends.

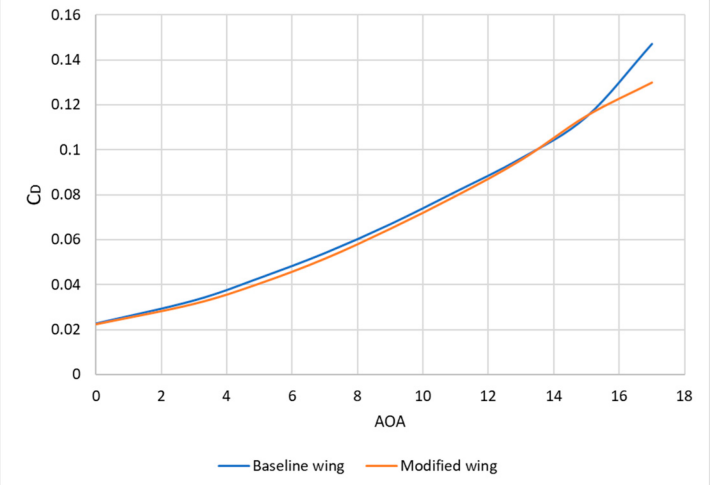

Figure 29. Comparison of the baseline and final wing drag coefficient trends.

Aerodynamic efficiency: Aerodynamic efficiency (C_L/C_D vs. AOA) provides the most accurate way of determining aerodynamic performance. Figure 30 compares the aerodynamic efficiency of the baseline wing and the final wing. An increased aerodynamic efficiency can be observed throughout the AOA regime (from 0° to stall angle). This means that both PFCDs complement one another and provide their respective benefits. The increased aerodynamic efficiency at lower angles of attack (0–10°) is due to the winglets, while MVGs contribute to the enhanced performance at the later angles of attack (10–15°), as demonstrated in Figure 30, by expressing the performance enhancement regions associated with the respective PFCDs. The maximum aerodynamic efficiency can be observed in the 0–4° AOA range, given the fact that the cruise angle of the UAV wing is chosen to be 4°.

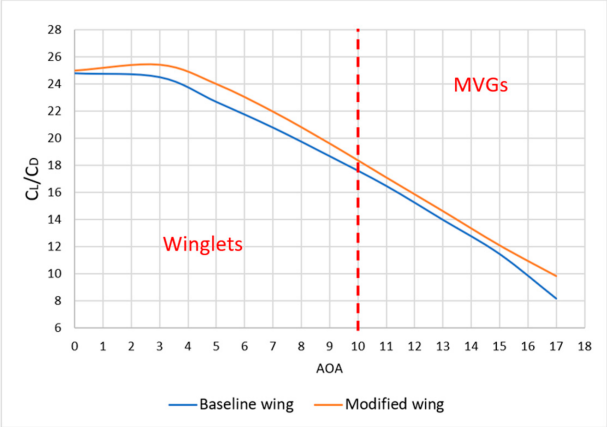

Figure 30. Comparison of the baseline and final wing aerodynamic efficiency.

Similar to the winglet cases, the non-dimensional improvement parameter described in Equation (3) was used for the numerical assessment of the performance enhancement of the final wing. Figure 31 illustrates the improvement percentage of the final wing with respect to the AOA. Compared to the baseline wing (horizontal line at 0%), a stable and continuous performance improvement can be observed at all angles of attack. The maximum improvement is within the 3–6° AOA range (up to 6%), which means that the cruise angle 4° of the planned UAV will fall in the main performance improvement zone. One important fact that needs to be explained is the sharp rise in the performance improvement parameter near the stall region. The stall angle of the final wing was delayed from 13° to 15° and, due to this reason (at 15°), the performance jumped to a much higher value as, by that time, the baseline wing had already stalled. This delayed stall and increased near-stall performance can be useful in special missions or situations where safety and maneuverability are essential. In such conditions, a UAV will stay stable for an extended time, especially in extreme flight conditions, such as sudden wind gusts.

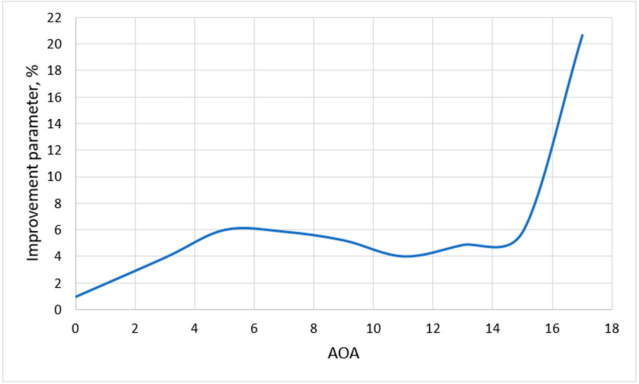

Figure 31. Lift-to-drag ratio enhancement of final wing.

4. Discussion and Conclusions

This investigative study tried to answer a unique question regarding the implementation of passive flow control devices (PFCDs) on small-scale low-speed UAVs. The use of winglets and Vortex Generators (VGs) for small-scale, low-speed UAVs is not very popular among researchers due to manufacturing complications and limited known benefits. The 4R-UAV project concerns innovations in aircraft/UAV designs and promoting green technologies in aviation. The project's two main objectives are green manufacturing (additive manufacturing) and aerodynamically improved designs for aircraft/UAV components. For small-scale UAV classes, 3D printing-based additive manufacturing techniques provide possibilities for improved designs and complex geometries without the usual restrictions of conventional manufacturing. Thanks to modern 3D printing and additive manufacturing techniques, the realization of PFCD-integrated wings, even for small-scale UAVs, has become possible.

In this work, two PFCDs (MVGs and winglets) were investigated for a small-scale UAV wing (span less than 2 m). Both the winglets and MVGs provided their benefits simultaneously. Regarding the feasibility of the PFCDs for small-scale low-speed UAV wings (which was the main question), this study provides a positive answer depending on the applications and mission requirements. Even though the improvement is limited, at this small-scale low-speed and low altitudes, 5–10% performance improvement is considerable. For example, for UAV missions where higher angles of attack are important for stability (military predator UAV types), MVGs are a good choice for performance improvement and delayed stall. Winglets, on the other hand, are good for cruise flight conditions at lower angles of attack, which in turn provides positive impact on UAV endurance. Depending on the users' requirements, the UAV can be equipped with either one of the PFCDs (winglets or MVGs) or both combined. In our case, future 4R-UAVs will be manufactured with wings integrated with both winglets and MVGs in order to gain the maximum aerodynamic advantage for all AOA ranges.

Following conclusions can be drawn from the study:

i. The computational based analysis of this study shows that PFCDs (Passive Flow Control Devices) are feasible for improving the aerodynamic performance of small-scale UAV wings.
ii. Both the PFCDs investigated in this study (winglets and MVGs) improved the aerodynamic performance specifically, during the cruise and near-stall conditions.
iii. The aerodynamic advantage (in terms of aerodynamic performance) achieved for the small-scale UAV's wing is limited, but can be advantageous for different mission requirements.
iv. MVGs (Micro Vortex Generators) enhanced the wing's near-stall properties, especially in terms of maximum lift coefficient (up to 6% increase) and stall delay (up to 2°).
v. Winglets (blended winglets, configuration 4 in this study) enhanced pre-stall properties by decreasing the drag (up to 10%) of the wing.
vi. PFCDs integrated to wing together, also provided a positive trend in performance improvement with nearly 6% aerodynamic efficiency in cruise conditions.
vii. Further investigations are planned in the future for the verification of the results by wind tunnel experiments and 4R-UAV flight testing.

Author Contributions: Conceptualization, A.A. and V.K.; methodology, A.A. and V.K.; software validation, V.K.; formal analysis, A.A. and V.K investigation, A.A. and V.K.; data curation, V.K.; writing—original draft preparation, A.A.; writing—review and editing, A.A.; visualization, V.K.; supervision, A.A.; project administration, A.A. All authors have read and agreed to the published version of the manuscript.

Funding: This work has been funded by the Latvian Council of Science, Fundamental and Applied Research Project, Project Nr. lzp-2021/1-0558.

Data Availability Statement: The data presented in this study are available on request from the corresponding author with restrictions as per the discretion of the funding body "Latvian Council of Science".

Acknowledgments: This work has been funded by the Latvian Council of Science, Fundamental and Applied Research Project, Project Nr. lzp-2021/1-0558. Project title: *Design and development of an aerodynamically efficient UAV (Unmanned Aerial Vehicle) by implementing the eco-friendly 4R circular economy concept in aviation: (4R-UAV).*

Conflicts of Interest: The authors declare no conflicts of interest.

References

1. European Commission. A European Green Deal. December 2019. Available online: https://ec.europa.eu/info/strategy/priorities-2019-2024/european-green-deal_en (accessed on 8 April 2024).
2. Wang, Z.; Zhuang, M. Leading-edge serrations for performance improvement on a vertical-axis wind turbine at low tip-speed-ratios. *Appl. Energy* **2017**, *208*, 1184–1197. [CrossRef]
3. Cai, C.; Zuo, Z.; Liu, S.; Maeda, T. Effect of a Single Leading-Edge Protuberance on NACA 634-021 Airfoil Performance. *J. Fluids Eng.* **2017**, *140*, 021108. [CrossRef]
4. Wei, Z.; New, T.H.; Cui, Y.D. An experimental study on flow separation control of hydrofoils with leading-edge tubercles at low Reynolds number. *Ocean Eng.* **2015**, *108*, 336–349. [CrossRef]
5. Kasper, W. Aircraft Wing with Vortex Generation. U.S. Patent No 3,831,885, 27 August 1974.
6. Olsman, W.F.J.; Colonius, T. Numerical simulation of flow over an airfoil with a cavity. *AIAA J.* **2011**, *49*, 143–149. [CrossRef]
7. Lam, G.C.Y.; Leung, R.C.K. Aeroacoustics of NACA 0018 airfoil with a cavity. *AIAA J.* **2018**, *56*, 4775–4786. [CrossRef]
8. Olsman, W.; Willems, J.; Hirschberg, A.; Colonius, T.; Trieling, R. Flow around a NACA0018 airfoil with a cavity and its dynamical response to acoustic forcing. *Exp. Fluids* **2011**, *51*, 493–509. [CrossRef]
9. Huebsch, W. Dynamic Surface Roughness for Aerodynamic Flow Control. In Proceedings of the 42nd AIAA Aerospace Sciences Meeting and Exhibit, Reno, NV, USA, 5–8 January 2004. [CrossRef]
10. Bai, T.; Liu, J.; Zhang, W.; Zou, Z. Effect of surface roughness on the aerodynamic performance of turbine blade cascade. *Propuls. Power Res.* **2014**, *3*, 82–89. [CrossRef]
11. Schubauer, G.B.; Spangenber, W.G. Forced Mixing in Boundary Layers. *J. Fluid Mech.* **1960**, *8*, 10–32. [CrossRef]
12. Jirásek, A. Design of vortex generator flow control in inlets. *J. Aircr.* **2006**, *43*, 1886–1892. [CrossRef]
13. Dol, S.S.; Pervaiz, S.S.; Uzair, M.; Khalid Bashir, S.; Elzughbi, M.M. Design of Solar-powered Endurance Glider with Vortex Generators. *Renew. Energy Res. Appl.* **2021**, *2*, 1–8. [CrossRef]
14. Arshad, A.; Kovaļčuks, V. Computational Investigations for the Application of Micro Vortex Generators (MVGs) for 4R-UAV Wing. In Proceedings of the IEEE Aerospace Conference, United States of America, Big Sky, MT, USA, 4–11 March 2023; pp. 1–6. [CrossRef]
15. Dagur, R.; Singh, V.; Grover, S.; Sethi, N.; Arora, B.B. Design of flying wing UAV and effect of winglets on its performance. *Int. J. Emerg. Technol. Adv. Eng.* **2018**, *8*, 414–428.
16. Panagiotou, P.; Kaparos, P.; Yakinthos, K. Winglet design and optimization for a MALE UAV using CFD. *J. Aerosp. Sci. Technol.* **2014**, *39*, 190–205. [CrossRef]
17. Turanoguz, E.; Alemdaroglu, N. Design of a medium range tactical UAV and improvement of its performance by using winglets. In Proceedings of the 2015 International Conference on Unmanned Aircraft Systems (ICUAS), Denver, CO, USA, 9–12 June 2015. [CrossRef]
18. Mestrinho, J.; Gamboa, P.; Santos, P. Design optimization of a variable-span morphing wing for a small UAV. In Proceedings of the 19th AIAA/ASME/AHS Adaptive Structures Conference, Denver, CO, USA, 4 April 2011. [CrossRef]
19. Arshad, A.; Kovaļčuks, V.; López, I.M. Application of SG6043mod airfoil for the enhanced aerodynamic characteristics of UAV wing. In Proceedings of the 10th International Conference on Recent Advances in Air and Space Technologies, Istanbul, Turkey, 7–9 June 2023.
20. Gigue're, P.; Selig, M.S. New airfoils for small horizontal axis wind turbines. *J. Sol. Energy Eng.* **1998**, *120*, 108–114. [CrossRef]
21. Xiong, Z.; Xu, Y.; Wang, Z.; Pian, X.; Wang, Y. Preliminary Design Method and Prototype Testing of a Novel Rotors Retractable Hybrid VTOL UAV. *IEEE Access* **2021**, *9*, 161141–161160. [CrossRef]
22. Raymer, D.P. *Aircraft Design: A Conceptual Approach. AIAA Education Series*, 6th ed.; Virginia Polytechnic Institute and State University Blacksburg: Blacksburg, VA, USA, 2018.
23. Kontogiannis, S.G.; Ekaterinaris, J.A. Design, performance evaluation and optimization of a UAV. *Aerosp. Sci. Technol.* **2013**, *29*, 339–350. [CrossRef]
24. Mueller-Vahl, H.; Pechlivanoglou, G.; Nayeri, C.N.; Paschereit, C.O. Vortex generators for wind turbine blades: A combined wind tunnel and wind turbine parametric study. In Proceedings of the ASME Turbo Expo, Turbine Technical Conference and Exposition, San Antonio, TX, USA, 3–7 June 2013; pp. 899–914.

25. Hu, J.; Niu, H.; Carrasco, J.; Lennox, B.; Arvin, F. Fault-tolerant cooperative navigation of networked UAV swarms for forest fire monitoring. *J. Aerosp. Sci. Technol.* **2022**, *123*, 107494. [CrossRef]
26. Weierman, J.; Jacob, J. Winglet design and optimization for UAVs. In Proceedings of the 28th AIAA Applied Aerodynamics Conference, Chicago, IL, USA, 28 June 2010.

Disclaimer/Publisher's Note: The statements, opinions and data contained in all publications are solely those of the individual author(s) and contributor(s) and not of MDPI and/or the editor(s). MDPI and/or the editor(s) disclaim responsibility for any injury to people or property resulting from any ideas, methods, instructions or products referred to in the content.